Metal-induced sensor mobilization turns on affinity to activate regulator for metal detoxification in live bacteria

Bing Fu[a,1], Kushal Sengupta[a,1], Lauren A. Genova[a,1], Ace George Santiago[a,2], Won Jung[a,3], Łukasz Krzemiński[a,4], Udit Kumar Chakraborty[a], Wenyao Zhang[a], and Peng Chen[a,5]

[a]Department of Chemistry and Chemical Biology, Cornell University, Ithaca, NY 14853

Edited by Ninian J. Blackburn, Oregon Health and Sciences University, Portland, OR, and accepted by Editorial Board Member Stephen J. Benkovic April 27, 2020 (received for review November 11, 2019)

Metal detoxification is essential for bacteria's survival in adverse environments and their pathogenesis in hosts. Understanding the underlying mechanisms is crucial for devising antibacterial treatments. In the Gram-negative bacterium *Escherichia coli*, membrane-bound sensor CusS and its response regulator CusR together regulate the transcription of the *cus* operon that plays important roles in cells' resistance to copper/silver, and they belong to the two-component systems (TCSs) that are ubiquitous across various organisms and regulate diverse cellular functions. In vitro protein reconstitution and associated biochemical/physical studies have provided significant insights into the functions and mechanisms of CusS–CusR and related TCSs. Such studies are challenging regarding multidomain membrane proteins like CusS and also lack the physiological environment, particularly the native spatial context of proteins inside a cell. Here, we use stroboscopic single-molecule imaging and tracking to probe the dynamic behaviors of both CusS and CusR in live cells, in combination with protein- or residue-specific genetic manipulations. We find that copper stress leads to a cellular protein concentration increase and a concurrent mobilization of CusS out of clustered states in the membrane. We show that the mobilized CusS has significant interactions with CusR for signal transduction and that CusS's affinity toward CusR switches on upon sensing copper at the interfacial metal-binding sites in CusS's periplasmic sensor domains, prior to ATP binding and autophosphorylation at CusS's cytoplasmic kinase domain(s). The observed CusS mobilization upon stimulation and its surprisingly early interaction with CusR likely ensure an efficient signal transduction by providing proper conformation and avoiding futile cross talks.

metal regulation | two-component system | protein interactions | signal transduction | single-molecule tracking

Maintaining metal homeostasis is critical for cells (1). Cells achieve this control through multiple mechanisms, including metal uptake, efflux, storage, and regulation pathways. Particularly, metal-sensing gene regulation enables cells to respond to metal stress or starvation efficiently (2, 3). In bacteria, metalloregulatory proteins can both sense (i.e., bind) metal ions and interact with DNA directly for transcriptional regulation (4–6). There are also two-component systems (TCSs), comprising a sensor and a response regulator that perform metal sensing and transcription regulation, respectively (2, 7, 8).

In the Gram-negative bacterium *Escherichia coli*, CusS–CusR is the TCS that regulates the *cus* operon that is responsible for *E. coli*'s Cu^+/Ag^+ tolerance in anaerobic growth and, under high copper stress, in aerobic growth (9–11). CusS is a homodimeric inner-membrane histidine kinase sensor; each monomer has a periplasmic sensor domain, transmembrane domain, and cytosolic kinase domain (12). CusR is the cognate cytosolic response regulator and has an N-terminal receiver domain that interacts with CusS and a C-terminal effector domain that binds DNA (13, 14). Once CusS binds Cu^+/Ag^+, its two periplasmic domains dimerize, and *cis*-autophosphorylation occurs at the H271 residue in the kinase domain. The activated CusS transfers the phosphoryl group to the D51 residue of CusR, which then dimerizes and binds tightly to the chromosomal CusR box to activate the transcription of *cusRS* and *cusCFBA* genes divergently, where *cusCFBA* encodes proteins for Cu^+/Ag^+ efflux (14–16). Besides CusS–CusR, TCSs across various organisms regulate genes of diverse functions (17), such as osmoregulation (EnvZ-OmpR) (18), chemotaxis (CheA-CheY) (19), and virulence activation (PhoQ/PhoP) (20). As in many TCSs, CusS–CusR is also susceptible to cross talks; e.g., CusR can be phosphorylated by other kinase sensors than CusS (21, 22).

Significance

How bacteria sense toxic chemicals and activate genes is crucial for their survival in adverse environments, including under antibacterial treatments. CusS, a membrane-localized sensor protein, and CusR, a response regulator protein, are key contributors to *Escherichia coli*'s resistance to the toxic metals copper and silver, and an example of the ubiquitous two-component gene regulation systems in bacteria. Using live-cell single-molecule imaging, we discovered a substrate-sensing–induced mobilization of the sensor protein in the cell membrane, which appears to be important for subsequent interaction with the regulator protein. We determined when sensor–regulator interaction affinity switches on after sensing the metal substrate; this timing appears to facilitate the efficiency of signal transduction events and is likely generalizable for other two-component systems.

Author contributions: B.F., K.S., and L.A.G. designed experiments, constructed strains, and performed biochemical experiments; B.F. and K.S. performed imaging experiments and analyzed data; B.F. wrote computer codes; A.G.S., W.J., Ł.K., U.K.C., and W.Z. contributed to strain construction, biochemical/imaging experiments, or data analyses/simulations; P.C. directed research; and B.F., K.S., L.A.G., and P.C. discussed results and wrote paper.

The authors declare no competing interest.

This article is a PNAS Direct Submission. N.J.B. is a guest editor invited by the Editorial Board.

Data deposition: Additional raw data and MATLAB codes have been deposited at Figshare (DOI: 10.6084/m9.figshare.11868639).

[1]B.F., K.S., and L.A.G. contributed equally to this work.

[2]Present address: Department of Microbiology and Immunobiology, Harvard Medical School, Boston, MA 02115.

[3]Present address: Department of Chemistry and Chemical Biology, Harvard University, Cambridge, MA 02138.

[4]Present address: Department of Biology, OncoArendi Therapeutics SA, 02-089 Warsaw, Poland.

[5]To whom correspondence may be addressed. Email: pc252@cornell.edu.

This article contains supporting information online at https://www.pnas.org/lookup/suppl/doi:10.1073/pnas.1919816117/-/DCSupplemental.

First published May 28, 2020.

In vitro studies of TCSs have contributed significantly to our present understanding of their molecular mechanisms (8, 14, 23). Studying purified proteins, while powerful and dissective, lacks the cellular environment. More important, the spatial context of proteins found inside a cell is abolished after reconstitution in vitro. For example, membrane proteins often cluster dynamically and localize spatially in the cell, leading to various mobilities that could bear different functions (24–28); whether this applies to CusS and what biological roles they may play are unknown. Measurements in live cells are needed to address these questions. Furthermore, the signal transduction from CusS to CusR comprises a series of molecular events: the binding of substrate (Cu^+/Ag^+) by CusS's periplasmic sensor domain, the allosteric signal propagation through its transmembrane domain to its cytosolic kinase domain for ATP hydrolysis and autophosphorylation, and the subsequent phosphoryl group transfer to CusR, which then binds to DNA to activate transcription (8, 12, 14, 29). It is poorly defined how different domains of CusS coordinate with one another and further with CusR in performing these events. Studying these coordinated molecular events requires full-length proteins of CusS and CusR, which are challenging to reconstitute in vitro, especially for multidomain membrane proteins like CusS (14).

Here, we report a single-molecule tracking (SMT) study of CusS–CusR in live *E. coli* cells via superresolution stroboscopic imaging. By tagging CusS and CusR with a photoconvertible fluorescent protein, we resolve and quantify their various mobility states under both copper-depleted and -stressed conditions, in combination with single-cell quantification of protein concentration (SCQPC) as well as genetic manipulations. We find that environmental copper stress leads to a cellular protein concentration increase and a concurrent mobilization of CusS out of clustered states in the inner membrane. The M133/M135 internal metal-binding sites in CusS's periplasmic sensor domains appear to play a role in CusS's mobilization. Importantly, mobilized CusS has significant interactions with CusR for signal transduction, in which CusS's affinity toward CusR switches on upon CusS binding copper at its interfacial metal-binding sites in the periplasmic sensor domains, prior to ATP binding and autophosphorylation at its cytoplasmic kinase domain(s). The timing of these molecular events appears to be advantageous to ensure efficient phosphoryl group transfer from autophosphorylated CusS to CusR during signal transduction for metal-sensing transcriptional regulation and could be broadly relevant to other TCSs in bacterial gene regulation.

Results and Analysis

SMT Identifies a Mobile and a Clustered Stationary State of CusS in the Membrane. To visualize CusS in live *E. coli* cells, we fused the photoconvertible fluorescent protein mEos3.2 (i.e., mE) (30) to its C terminus at its chromosomal locus, creating $CusS^{mE}$ at a physiological expression level. Using cells that also express $CusS^{mE}$ from a plasmid to increase cellular protein level, Western blot shows that $CusS^{mE}$ is largely intact (<11% cleavage of the mE tag; *SI Appendix*, Fig. S6), and confocal microscopy of these cells further confirms $CusS^{mE}$'s membrane localization, where some cells show protein aggregation, likely due to protein overexpression (Fig. 1*A* and *SI Appendix*, Fig. S3) (*SI Appendix*, section 1.6). Cell growth assays [using a Δ*cueO* base strain to increase cells' sensitivity to copper stress (9–11)] further show that $CusS^{mE}$ is as functional as the untagged CusS in conferring cell resistance to copper (*SI Appendix*, Fig. S5*B*).

Using sparse photoconversion and time-lapse stroboscopic fluorescence imaging (4-ms laser exposure; 60-ms time lapse) (31, 32), we tracked the motions of single $CusS^{mE}$ proteins in live cells with tens of nanometer precision until their mE tags photobleached (Fig. 1*B*, *Inset*, and *SI Appendix*, section 1.4). Cells are viable under our imaging conditions (32). This SMT gives the probability distribution function (PDF) of the displacement length r per time lapse, which, although containing rich information about the diffusive behaviors of $CusS^{mE}$, is distorted because of the confinement effect from a 2D projection of diffusion on the curved cell membrane surface. We therefore performed ITCDD (inverse transformation of confined displacement distribution) (33–35) to deconvolute this confinement effect (Fig. 1*B* and *SI Appendix*, section 4.1).

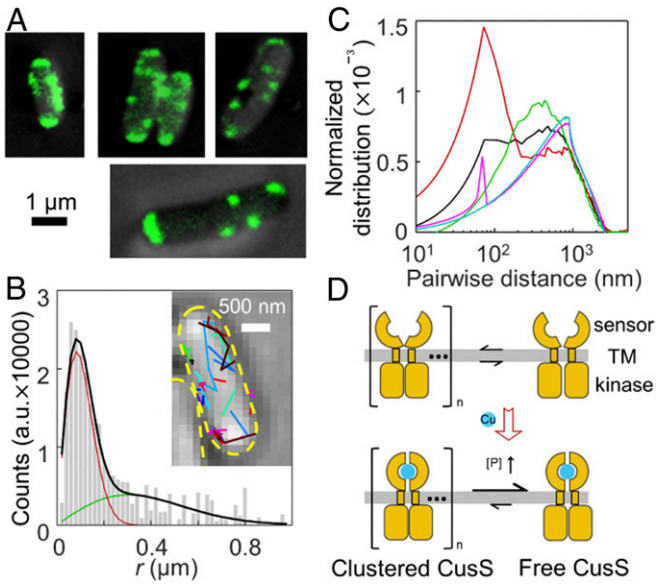

Fig. 1. SMT resolves two states of CusS in the membrane. (*A*) Confocal fluorescence images of cells overexpressing $CusS^{mE}$. (*B*) ITCDD-corrected distribution of displacement length r of $CusS^{mE}$ from 17,029 molecules and 1,282 cells grown in copper-depleted medium. Lines: overall fit (black) and the resolved quasistationary (red) and mobile (green) diffusion states. The y axis is not the actual counts of displacement lengths; it only represents the relative probabilities of different displacement lengths due to ITCDD correction. (*Inset*) Typical tracking trajectories in a cell overlaid on its bright-field transmission image. Dashed yellow lines: cell boundaries. (*C*) Pairwise distance distribution (PWDD) of first locations of $CusS^{mE}$ tracks. Black, all $CusS^{mE}$ molecules; red, quasistationary molecules; green, mobile molecules; blue, simulated randomly positioned molecules on cell membrane; magenta, simulated randomly positioned dimers on cell membrane (*SI Appendix*, section 5). (*D*) Schematic of copper stress-induced mobilization of CusS in the membrane. (*Top*) Quasistationary (clustered) and mobile (free) CusS dimers at a dynamic equilibrium. (*Bottom*) CusS's periplasmic sensor domains dimerize and CusS protein concentration ([P]) increases upon copper stress; higher [P] and copper binding both shift the equilibrium toward the mobile state. TM, transmembrane domain.

For cells grown in copper-depleted medium (nutrient-supplemented M9, 0.011 ± 0.002 μM residual Cu; *SI Appendix*, Table S4), the ITCDD-corrected PDF(r) is sufficiently fitted by two diffusion states (Fig. 1*B* and *SI Appendix*, section 4.1): a mobile, faster state with diffusion constant (D_m) of 0.93 ± 0.06 $\mu m^2 \cdot s^{-1}$ and fractional population (A_m) of 36 ± 2%; and a much slower state with diffusion constant (D_s) of 0.054 ± 0.003 $\mu m^2 \cdot s^{-1}$ and fractional population (A_s) of 64 ± 2%. This slower state is quasistationary because D_s is only slightly larger than the apparent diffusion constant (~0.01 $\mu m^2 \cdot s^{-1}$) for a stationary molecule considering our ~40-nm localization uncertainties (*SI Appendix*, section 4.3).

We assigned the mobile state to $CusS^{mE}$ dimers freely diffusing in the inner membrane (Fig. 1*D*, *Top Right*) because, first, free CusS dimers are expected to exist (CusS is intrinsically dimeric ref. 12), and second, the diffusion constant D_m is comparable to those of mobile membrane proteins (35–37). We attributed the quasistationary state to $CusS^{mE}$ dimers clustered

together (either directly or in association with other proteins) (Fig. 1*D*, *Top Left*), considering that membrane proteins can form clusters with reduced mobility (27, 28). To support the assignment of this clustered state, we examined the distribution of pairwise distances between the first locations of each tracked $CusS^{mE}$ (black curve, Fig. 1*C*). A small peak is clearly visible at a short distance of ∼70 nm, supporting the presence of $CusS^{mE}$ protein clusters, whereas simulations of proteins distributed randomly on the membrane do not show such a peak (blue curve, Fig. 1*C* and *SI Appendix*, section 5). We further separated these first locations into two categories: those associated with displacements smaller than a threshold displacement r_0 (∼166 nm, *SI Appendix*, section 5), which would be dominated by $CusS^{mE}$ in the quasistationary state (Fig. 1*B* and *SI Appendix*, Fig. S7*A*), and those associated with displacements larger than this threshold, which would be dominated by $CusS^{mE}$ in the mobile free dimer state. Strikingly, the pairwise distance distribution (PWDD) from locations dominantly in the mobile state does not show any discernible peak in the <100-nm distance range (green, Fig. 1*C*), whereas that for the quasistationary state has a pronounced peak at ∼70 nm (red, Fig. 1*C*). The PWDD of simulated randomly positioned dimers (where the intermonomer distance was artificially set to 70 nm; *SI Appendix*, section 5) shows a peak at ∼70 nm (magenta, Fig. 1*C*), whose amplitude is much smaller than that for the quasistationary molecules in the experiment (red). Therefore, this pronounced peak (red) cannot merely come from the dimeric nature of CusS, further supporting the assignment of the quasistationary state to $CusS^{mE}$ clusters.

Copper Stress Leads to CusS Concentration Increase and Mobilization in the Membrane. We performed SCQPC (32) to determine the total $CusS^{mE}$ protein concentration in each cell ($[CusS^{mE}]$, in terms of monomers; *SI Appendix*, section 1.4). In copper-depleted medium, the physiological $[CusS^{mE}]$ is heterogeneous and ranges from ∼47 to 476 nM, averaging at ∼167 ± 80 nM (Fig. 2*A*). We then sorted cells into groups, with each group having a similar $[CusS^{mE}]$, to deconvolute protein concentration heterogeneity in analyzing the displacement distributions. Regardless of $[CusS^{mE}]$, the same two diffusion states are resolved in each group: the mobile state and the quasistationary state with diffusion constants of 0.97 ± 0.13 $\mu m^2 \cdot s^{-1}$ (D_m) and 0.05 ± 0.01 $\mu m^2 \cdot s^{-1}$ (D_s), respectively, when globally fitted (*SI Appendix*, section 4.4).

In the presence of steady 2 mM Cu^{2+} stress in the medium, a level that was shown to induce significant CusS protein expression in the cell (38) and inhibit cell growth in strains lacking the *cusS* gene (12), the distribution of cellular $[CusS^{mE}]$ broadens significantly toward higher concentrations, reaching up to ∼950 nM for some cells and averaging at ∼312 ± 120 nM, which is ∼2-fold higher than that in the absence of copper stress (Fig. 2*A*). This protein level increase probably results mainly from transcriptional activation of the *cus* gene and less from posttranscriptional activation because the mRNA level of *cusS* gene increases by a similar ∼2.2-fold upon copper stress (*SI Appendix*, section 1.7 and Fig. S4). Note that this increase in $[CusS^{mE}]$ happens gradually over a period of ∼2 h after introducing copper stress (*SI Appendix*, Fig. S22), reflecting that it takes time from transcription to protein synthesis [maturation of the mE tag is faster, at ∼20 min (30)]. Across this larger range of $[CusS^{mE}]$, the fractional population A_m of the mobile state increases significantly from ∼30% to ∼70% (i.e., more than doubles), with a concurrent decrease of A_s for the quasistationary state (Fig. 2*B*, open symbols), while both states increase in absolute concentration (e.g., mobile state increases from ∼33 to ∼557 nM; *SI Appendix*, Fig. S21). (Note that the highest $[CusS^{mE}]$ data point in Fig. 2*B* is not reliable because few cells have such high protein concentrations.) Moreover, at any fixed particular $[CusS^{mE}]$, the 2 mM Cu^{2+} stress increases A_m by a factor of ∼1.3 (e.g., comparing open vs. solid green triangles vertically at ∼200 nM $CusS^{mE}$; Fig. 2*B*). Altogether, these results show that copper stress leads to a significant mobilization of CusS in the cell membrane, which results more from an increase of overall cellular CusS concentration (more than 2-fold) and less from direct copper binding to CusS proteins (only ∼1.3-fold).

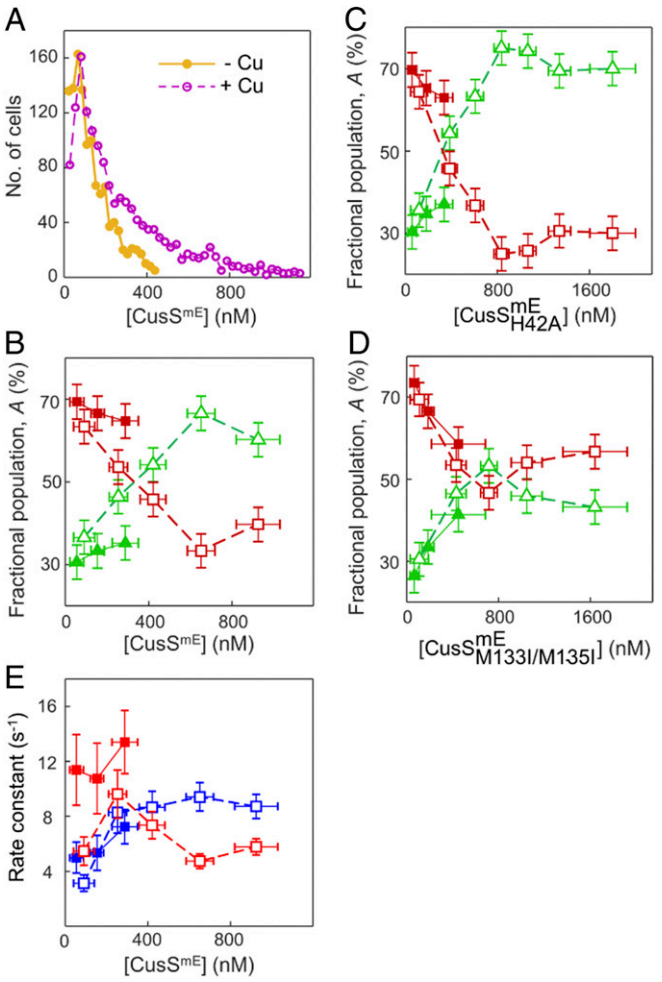

Fig. 2. (*A*) Distribution of cellular $CusS^{mE}$ concentration $[CusS^{mE}]$ (all in terms of monomeric CusS) in the absence or presence of 2 mM Cu^{2+} stress. (*B–D*) Fractional populations (*A*'s) of mobile (green) and quasistationary (red) states of $CusS^{mE}$ in the absence (solid symbols) or presence (open symbols) of 2 mM Cu^{2+} stress vs. $[CusS^{mE}]$ in WT (*B*), $CusS^{mE}_{H42A}$ (*C*), and $CusS^{mE}_{M133I/M135I}$ strains (*D*). The *x* error bars are SDs of protein concentration; *y* error bars are SDs of *A* from bootstrapping (*SI Appendix*, section 4.4). (*E*) Interconversion rate constants between the stationary and mobile states of $CusS^{mE}$. k_d: declustering rates from the stationary state, blue; k_c: clustering rates from the mobile state, red. Solid, 0 mM Cu^{2+}; dashed, 2 mM Cu^{2+} stress. For calculations on k_d and k_c, see *SI Appendix*, section 6.

Previous studies have shown that dimeric CusS can bind Cu^+/Ag^+ at two types of sites in its periplasmic domains (12): at two interfacial sites [each with Phe43 and His176 from one monomer and His42 from the other monomer as ligands; K_d ∼8 μM for Ag^+ (29)] that leads to the dimerization of the two periplasmic domains and the activation of CusS's downstream signaling; and at two internal sites (each with Met133, Met135, His145, and Ser84 as ligands) that are not conserved across different organisms and appear insignificant for cell viability under copper stress (12). To probe whether copper binding at the interfacial or internal sites is relevant to the observed CusS mobilization in the

membrane, we first mutated $CusS^{mE}$'s His42 to alanine, which should abolish its copper binding at the interfacial sites and was shown to abolish CusS autophosphorylation and impair cell's resistance to copper stress (*SI Appendix*, Fig. S5) (12, 14). The behaviors of this $CusS^{mE}_{H42A}$ mutant are similar to $CusS^{mE}$ with or without copper stress (Fig. 2*C* vs. Fig. 2*B*), including the increase in cellular CusS concentration upon copper stress as well as the significant mobilization with increasing [$CusS^{mE}_{H42A}$] and at any particular [$CusS^{mE}_{H42A}$]. This similarity strongly suggests that copper binding at the interfacial sites, although important for CusS activation, has no significant contribution to CusS mobilization in the membrane. The copper stress-induced $CusS^{mE}_{H42A}$ concentration increase is surprising here, as this H42A mutation abolishes the activation of CusS, which autoregulates itself; we attribute this protein concentration increase to cross-activations of *cusRS* regulon by other regulatory pathways (22).

Alternatively, we performed an M133I/M135I double mutation on $CusS^{mE}$ to abolish copper binding at the internal sites. As reported previously (12), these mutations do not give phenotypical changes in cells' resistance to copper stress (*SI Appendix*, Fig. S5). Without copper stress, this $CusS^{mE}_{M133I/M135I}$ mutant behaves similarly to $CusS^{mE}$ (Fig. 2*D* vs. Fig. 2*B*, solid symbols). However, in the presence of 2 mM Cu^{2+}, A_m only increases to ∼50%, significantly smaller than the ∼70% for $CusS^{mE}$, even though the protein concentration range reaches high levels (Fig. 2*D* vs. Fig. 2*B*, open green triangles). Moreover, at any particular CusS concentration (i.e., comparing data vertically in Fig. 2*D*), the copper-induced mobilization (i.e., increase in A_m) vanishes. Altogether, these results suggest that copper binding at the internal sites of CusS, albeit having no phenotypic consequences, plays a role in copper-induced CusS mobilization in the cell membrane, perhaps via inducing CusS conformational changes.

We further studied the diffusion dynamics of $CusS^{mE}$ in a Δ*cusR* deletion strain. Two-state diffusion behaviors were similarly observed (*SI Appendix*, Fig. S24), indicating that the protein concentration-induced and copper-induced mobilization of CusS is unrelated to CusR. The copper-induced CusS concentration increase in this Δ*cusR* strain (as also observed in $CusS^{mE}_{H42A}$) again indicates that accumulation of CusS can be independent of a functional CusS–CusR regulatory circuit and here likely comes from cross-activation via other regulatory pathways (22).

Mobile and Clustered States of CusS Are in Dynamic Exchange. To probe whether the mobile free $CusS^{mE}$ dimers and their quasistationary clusters can exchange dynamically, we examined the interconversion kinetics between these two states (*SI Appendix*, section 6). Here, we analyzed the displacement length-vs.-time trajectories of single $CusS^{mE}$ in the cell, obtainable from the tracking trajectories as in Fig. 1*B*, *Inset*. Thresholding these displacement trajectories with an upper displacement limit (determined from the diffusion constant of the quasistationary state) selects out those small displacements and provides the estimate of the individual residence times τ of a single $CusS^{mE}$ dimer within the clusters (*SI Appendix*, Fig. S17*A*). By analyzing the distribution of τ and correcting for the photobleaching/blinking kinetics of the mE tag (*SI Appendix*, Fig. S17*B*), and using a validated quasiequilibrium two-state kinetic model between the mobile and clustered states (*SI Appendix*, Fig. S17*C*), we obtained k_d and k_c, the two apparent first-order rate constants of $CusS^{mE}$ leaving and entering the clustered state, respectively, as a function of [$CusS^{mE}$].

k_d and k_c are on the order of 10^0 to 10^1 s^{-1}, corresponding to an interconversion timescale of 10^{-1} to 10^0 s between the mobile free $CusS^{mE}$ and the quasistationary clusters (Fig. 2*E*). This interconversion timescale is also 1,000 times faster than the typical protein lifetime of ∼1,200 min in bacteria (39–42), indicating that these two states are in dynamic exchange (Fig. 1*D*) and cannot be from different-aged CusS proteins in the cell (e.g., newly synthesized vs. partially degraded/aggregated). Moreover, under copper stress and with increasing [$CusS^{mE}$], k_d, the declustering rate constant increases (Fig. 2*E*, open blue squares), consistent with the mobilization of CusS in the membrane. An independent analysis using hidden Markov models shows consistent results (*SI Appendix*, Fig. S18*C* and section 6). The dynamic exchange between the two diffusion states are also observed for $CusS^{mE}_{H42A}$ and $CusS^{mE}_{M133I/M135I}$ (*SI Appendix*, Fig. S17 *E* and *F*).

Mobilized CusS Interacts with CusR upon Copper Stress. We postulated that the mobilized, free dimer state of CusS in the membrane should be functionally important for interacting with CusR for signal transduction because of the following: First, significant mobilization of CusS was observed only after copper stress (Fig. 2*B*). Second, the major contributor to this enhanced mobilization is the increase in [CusS] in the cell, which is again a result of copper stress. Third, the physiological function of CusS is to sense copper (and silver) stress and transduce the signal to CusR. To test this postulate, we imaged in cells the dynamic behaviors of $CusR^{mE}$, which carries a C-terminal mEos3.2 tag encoded at CusR's chromosomal locus. It is worth noting that in making this fusion, we considered the 11 base pair overlap between *cusR* and *cusS* genes so that the strain still contains an intact CusS (*SI Appendix*, section 1.1). Cell growth assays and Western blot show that $CusR^{mE}$ is as functional as the untagged CusR in conferring cell copper resistance and is largely intact with <9% cleavage of the tag (*SI Appendix*, Figs. S5 and S6).

We then performed SMT of $CusR^{mE}$ along with SCQPC to quantify its concentration in each cell ([$CusR^{mE}$]). Grown in copper-depleted medium, the cellular [$CusR^{mE}$] (in terms of monomers) ranges from ∼33 to 600 nM, averaging at 167 ± 42 nM (Fig. 3*A*), consistent with a previous immunoblotting study (8). Under 2 mM Cu^{2+} steady stress, [$CusR^{mE}$] increases expectedly, averaging at 285 ± 110 nM, but could reach ∼1,100 nM for some cells (Fig. 3*A*).

We again sorted cells into groups of similar [$CusR^{mE}$] and analyzed ITCDD-corrected displacement length distributions to extract the minimal number of diffusion states, as well as their corresponding diffusion constants and fractional populations. At any cellular [$CusR^{mE}$], three states are resolved (e.g., Fig. 3*B*). Under copper-depleted conditions, the fastest diffusion state has a diffusion constant D_{FD} of 7.9 ± 0.6 $\mu m^2 \cdot s^{-1}$, which we assigned as $CusR^{mE}$ freely diffusing (FD) in the cytoplasm (either as monomers or dimers), as these species are expected to exist and D_{FD} is consistent with those for freely diffusing proteins in the bacterial cytoplasm (34, 43, 44). The slowest state has a diffusion constant D_{TB} of 0.02 ± 0.01 $\mu m^2 \cdot s^{-1}$, which we assigned as $CusR^{mE}$ tightly bound (TB) to the chromosome because CusR, when phosphorylated (i.e., activated), can bind tightly at cognate sites; D_{TB} is also consistent with those for proteins that bind chromosome specifically (31, 34, 45, 46), and its small magnitude mainly reflects chromosomal dynamics and experimental uncertainties in molecular localization. This TB state may or may not have contributions from $CusR^{mE}$ interacting with the quasistationary state of CusS, which has a similar diffusion constant (∼0.05 $\mu m^2 \cdot s^{-1}$). With increasing cellular [$CusR^{mE}$], the fractional population A_{FD} of the freely diffusing state increases expectedly (Fig. 3*C*, solid blue squares), while A_{TB} of the tightly bound state decreases, which is also expected as there are a limited number of sites on chromosome for $CusR^{mE}$ to bind tightly (Fig. 3*C*, solid red squares); both trends support the assignments of these two states. The third, intermediate (IN) diffusion state has a diffusion constant D_{IN} in the range of 0.24 to 0.33 $\mu m^2 \cdot s^{-1}$ (Fig. 3*E*, solid green); we attributed this state to having contributions from $CusR^{mE}$ nonspecifically bound to the chromosome [which is expected to occur,

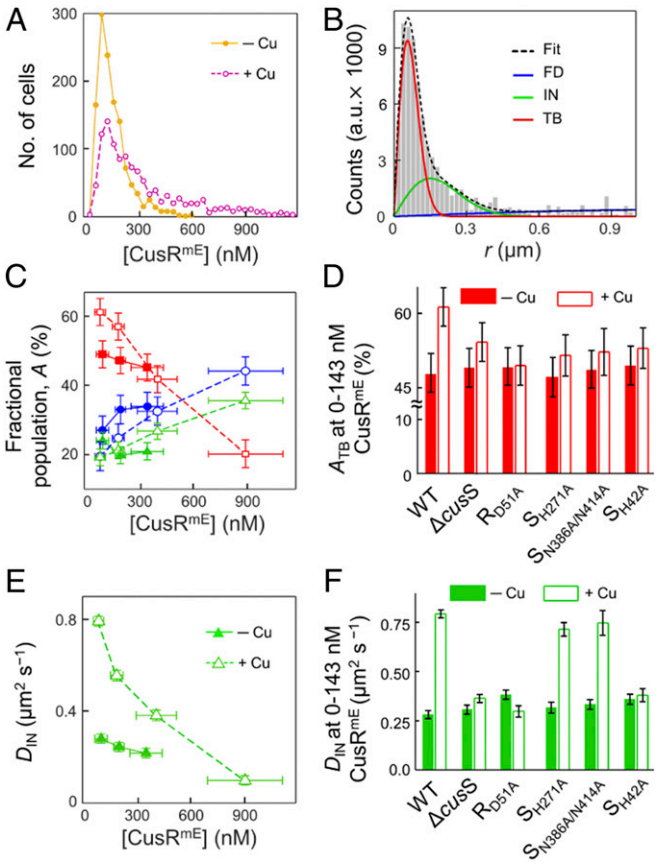

Fig. 3. SMT reveals CusR interaction with the mobile state CusS upon copper stress. (*A*) Distribution of cellular $CusR^{mE}$ concentration (in monomers) in the WT $CusR^{mE}$ strain in the absence or presence of 2 mM Cu^{2+} stress. (*B*) ITCDD-corrected distribution of displacement length *r* at $[CusR^{mE}]$ = 167 ± 12 nM in WT cells under copper-depleted condition. Black dotted line: overall fit; solid lines: the resolved freely diffusing (FD) (blue), intermediate (IN) (green), and tightly bound (TB) (red) diffusion states. (*C* and *E*) Fractional populations of the three diffusion states (*C*) and diffusion constants of the IN state (*E*) vs. $[CusR^{mE}]$ in WT cells under copper-depleted (solid symbols) and copper-stress conditions (open symbols). Blue, green, and red: FD, IN, and TB states, respectively. (*D* and *F*) Fractional populations of the TB state (*D*) and diffusion constants of the IN state (*F*) at low cellular $[CusR^{mE}]$ (i.e., ~0 to 143 nM) in various CusR mE-tagged strains under copper-depleted/stress conditions. Please note the break in the *y* axis in *D*. Error bars are SD.

and the magnitude of D_{IN} is consistent with reports (31)] and possibly from interactions with the mobile state of CusS, the two of which are not resolved here.

Under copper stress, the diffusion constants D_{FD} and D_{TB} of the freely diffusing and tightly bound states remain almost unchanged from those under copper-depleted conditions and subsequently were globally fitted across $[CusR^{mE}]$ groups (*SI Appendix*, section 4.4). Importantly, the fractional population A_{TB} of the tightly bound state increases upon copper stress, especially at low $[CusR^{mE}]$—at ~83 nM, A_{TB} increases from ~47% to ~62% (Fig. 3*C*, solid vs. open red squares)—consistent with that upon copper stress, there should be more phosphorylated (i.e., activated) $CusR^{mE}$, which can bind the chromosome tightly. More interestingly, at the low end of cellular $[CusR^{mE}]$ range, the value of the intermediate diffusion state D_{IN} is 0.80 ± 0.02 $\mu m^2 \cdot s^{-1}$ (Fig. 3*E*, open triangles), much larger than under copper-depleted conditions and close to the diffusion constant of the mobile CusS state (0.97 ± 0.13 $\mu m^2 \cdot s^{-1}$, Fig. 1*B*). We attributed this larger D_{IN} here to a significantly increased interaction of CusR with mobile CusS under copper stress. This attribution is consistent with expectation that, under copper stress, CusS affinity for CusR should increase to recruit CusR for phosphorylation and subsequent signal transduction. Notably, this copper stress-induced increase in D_{IN} diminishes with increasing cellular $[CusR^{mE}]$ (Fig. 3*E*, open triangles), suggesting that at higher $[CusR^{mE}]$, this intermediate state becomes dominated by nonspecific interactions with the chromosome rather than with mobile CusS (see discussion in *SI Appendix*, section 6).

To further validate the assignments of the diffusion states of $CusR^{mE}$ in cells, we examined CusR's behavior in two control strains. The first is a Δ*cusS* strain, in which no CusS-to-CusR signal transduction is possible (*SI Appendix*, Fig. S5). Here, SMT still resolved the three diffusion states of $CusR^{mE}$. However, at the low ~70 nM cellular $[CusR^{mE}]$, the copper stress-induced increase in A_{TB} is diminished compared with the wild-type (WT) $CusR^{mE}$ strain (Fig. 3*D*, columns 3 and 4 vs. 1 and 2), consistent with that no CusS is present to phosphorylate and activate CusR for subsequent tight binding to chromosome. The residual small increase in A_{TB} is attributable to CusR phosphorylation via cross-talks by other sensor kinases (22, 47) (*Discussion*). More important, the copper stress-induced increase in D_{IN} of the intermediate state in the low protein concentration region, as observed in the WT $CusR^{mE}$ strain, vanished in the Δ*cusS* strain (Fig. 3*F*, columns 3 and 4 vs. 1 and 2), strongly supporting that this increase in D_{IN} in the WT strain reflects CusR interactions with CusS, more specifically with the mobile state of CusS, where the interactions switch on upon copper stress.

The second control strain harbors a phosphorylation site mutation D51A on $CusR^{mE}$ (i.e., $CusR^{mE}_{D51A}$), so that CusR cannot be phosphorylated/activated (*SI Appendix*, Fig. S5) (14). Past studies (48–51) on other TCS systems showed that this type of mutation on response regulators also alters their conformations and impairs their interactions with sensor kinases. No increase in A_{TB} was observed upon copper stress (Fig. 3*D*, columns 5 and 6), consistent with that $CusR^{mE}_{D51A}$ cannot be phosphorylated (not even via cross talks here) to increase its DNA binding affinity. Moreover, the increase in D_{IN} upon copper stress also vanished (Fig. 3*F*, columns 5 and 6 vs. 1 and 2), further supporting our assignment of its origin in the WT strain, because $CusR^{mE}_{D51A}$ was expected to not interact with CusS.

Interestingly, $CusR^{mE}_{D51A}$ always has a significant fractional population A_{TB} of the tightly bound state to the chromosome (e.g., ~50% at low CusR concentration), comparable to that for WT $CusR^{mE}$ under copper-depleted conditions, in which the unphosphorylated form should be a significant component of cellular CusR (Fig. 3*D*, columns 5 and 6 vs. 1). This comparability directly suggests that unphosphorylated CusR can also bind DNA tightly (although not as strongly as the phosphorylated form), consistent with reports on unphosphorylated forms of other response regulators (52–54) (this binding does not lead to gene activation, however, possibly due to wrong interaction conformations).

CusS's Affinity toward CusR Switches on upon Sensing Copper at Its Sensor Domain Prior to ATP Binding and Autophosphorylation at Its Kinase Domain. The pathway from CusS sensing copper (or silver) to the eventual phosphorylation and activation of CusR comprises a sequence of events (14) (Fig. 4): *i*) copper binding at the interfacial sites in CusS's periplasmic sensor domains, leading to sensor domain dimerization and allosteric conformational changes in the cytoplasmic kinase domains; *ii*) ATP binding at the kinase domains; *iii*) *cis*-autophosphorylation of the kinase domain H271 residue (14); and *iv*) phosphoryl group transfer to the D51 residue on CusR, activating CusR for subsequent binding to chromosomal operator site.

We have shown that, upon copper stress, CusR interacts significantly with the mobile state of CusS. To probe where among the sequence of events this interaction affinity switches on, we first mutated the autophosphorylation site H271 at CusS's kinase domain to alanine (i.e., $CusS_{H271A}$), eliminating step *iii*, the last step before phosphoryl group transfer to CusR, and imaged the behaviors of $CusR^{mE}$ in cells. SMT shows that upon copper stress, the increase in the fractional population A_{TB} of tightly bound state to chromosome is much less compared with the WT $CusR^{mE}$ (Fig. 3*D*, columns 7 and 8 vs. 1 and 2), consistent with that $CusS_{H271A}$ cannot phosphorylate CusR, leaving only CusR phosphorylation via cross-talk mechanisms for subsequent chromosomal binding, similar to the behavior of the Δ*cusS* strain. However, unlike the Δ*cusS* strain, D_{IN}, the diffusion constant of the intermediate state that contains CusR interaction with the mobile CusS, still increases (as in the WT $CusR^{mE}$ strain) upon copper stress (Fig. 3*F*, columns 7 and 8 vs. 1 and 2), indicating that mobile CusS can interact with CusR even without autophosphorylation.

We then made N386A/N414A double mutations in CusS's kinase domain to abolish its ATP binding (14) (i.e., step *ii*; Fig. 4). Upon copper stress, similar behaviors of $CusR^{mE}$ were observed as in the above $CusS_{H271A}$ strain especially the increase in D_{IN} (Fig. 3*F*, columns 9 and 10 vs. 1 and 2). These results indicate that copper-induced CusR–CusS interactions are still feasible even without ATP binding to CusS.

Finally, we made an H42A mutation at CusS's interfacial metal-binding sites in its periplasmic sensor domains, abolishing CusS's copper sensing (step *i* in Fig. 4) and examined $CusR^{mE}$. Upon copper stress, there is a small increase in the tight DNA binding population (A_{TB}) (Fig. 3*D*, columns 11 and 12), as expected for the same cross-talk mechanism. Strikingly, there is no increase in D_{IN} (Fig. 3*F*, columns 11 and 12), as in the Δ*cusS* strain, reflecting no significant interactions between CusR and mobile $CusS_{H42A}$. Altogether, these results show that within the CusS-to-CusR signal transduction pathway, significant CusS–CusR interaction switches on as soon as CusS senses copper and before CusS undergoes subsequent ATP binding and autophosphorylation.

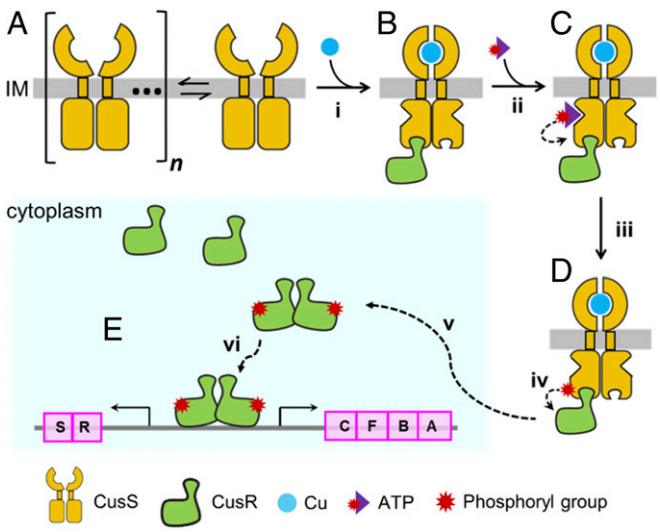

Fig. 4. Schematic of CusS-to-CusR signal transduction in cells upon sensing copper, showing (*A*) the two-state equilibrium of CusS in the inner membrane (IM); (*B*) CusS's mobilization upon binding copper at its periplasmic sensor domain, and the recruitment of CusR; (*C*) ATP binding to CusS's cytoplasmic kinase domain and its autophosphorylation; (*D*) phosphoryl group transfer to the bound CusR; and (*E*) the eventual binding of phosphorylated CusR to chromosomal operator site for transcription activation.

Discussion

We have imaged in live cells the spatiotemporal dynamics of membrane sensor CusS and response regulator CusR of the two-component sensor–regulator system for the *cus* operon that helps *E. coli* resist copper/silver toxicity through efflux. We found that CusS exists dominantly in two diffusive states that are in dynamic exchange (Figs. 1*D* and 4*A*). The quasistationary state of CusS is attributable to clustered dimers in the inner membrane, whose existence could stem from natural affinities of CusS dimers toward each other or from association with other cellular proteins; this type of clustering is often observed for membrane proteins in bacteria (27, 28). The mobile state of CusS is attributable to free dimers diffusing in the membrane; this mobile state increases not only in absolute population but also in fractional population upon stressing the cell with copper in the medium (Fig. 2*B*). This copper stress-induced CusS mobilization has two contributors. The major contributor is the overall increase of the cellular CusS concentration, expected from copper-induced activation of *cusS* gene expression. Increase in overall protein concentration should increase the absolute population of the mobilized CusS, but the increase in its fractional population is nonintuitive. Using a simple clustering equilibrium model, we found that this protein concentration-induced mobilization could come from a reduction in apparent affinity between CusS dimers or a change of cluster size in the membrane (*SI Appendix*, section 8 and Fig. S20). The minor contributor is copper binding to the internal sites in CusS's periplasmic domains; here copper-binding–induced conformational changes might decrease inter-dimer interactions, leading to CusS mobilization from the clustered state.

Interestingly, we discovered that CusR interacts with the mobile state of CusS, supporting the physiological significance in cellular signal transduction for CusS mobilization upon copper stress. Possibly, the mobile CusS has more freedom to adopt suitable conformations to interact with CusR for signal transduction. It is worth noting that although higher mobility may be perceived to increase CusS's collision probability with CusR, this idea is likely invalid here. This is because the frequency of diffusional collisions is dominated by the faster-moving component of interacting partners (*SI Appendix*, section 7); and for the CusS–CusR interaction, it is dominated by CusR in the cytosol ($D_{FD} \sim 7.9\ \mu m^2 \cdot s^{-1}$), which is eight times faster than the mobile CusS in the membrane ($D_m \sim 0.97\ \mu m^2 \cdot s^{-1}$).

Moreover, we found that the interaction affinity of the mobile CusS toward CusR switches on as soon as CusS's periplasmic sensor domains bind copper (Fig. 4*B*), prior to ATP binding at the cytoplasmic kinase domain(s) (Fig. 4*C*) and autophosphorylation at the H271 site (Fig. 4*D*). The timing of gaining this affinity is likely advantageous for the following reasons. First, ATP binding is known to be reversible and facile (Fig. 4, step *ii*) [e.g., ATP unbinding rate is $\sim 10^0\ s^{-1}$ for the catalytic domain of CheA, a histidine kinase for chemotaxis signal transduction (55)], whereas the subsequent autophosphorylation is much slower (i.e., lower in probability) (Fig. 4, step *iii*) [e.g., autophosphorylation is $\sim 10^{-2}\ s^{-1}$ for DesK, a histidine kinase in the DesKR TCS that senses changes in membrane fluidity in *Bacillus subtilis*, and for WalK, a histidine kinase in the WalKR TCS that maintains cell wall homeostasis in *Streptococcus pneumonia* (56, 57)]. It would thus be preferable for CusR to be recruited to CusS earlier and stay bound, waiting for the less probable autophosphorylation to occur while the ATP binds/unbinds reversibly. Second, the phosphohistidines of membrane sensors are high-energy species [e.g., phosphoryl group transfer is $\sim 10^1\ s^{-1}$ for the VanRS TCS that provides vancomycin resistance in *Enterococci* (56, 58)]. Here, having CusR already bound to CusS's kinase domain and ready to accept the phosphoryl group (Fig. 4,

step *iv*) would help avoid the decay of the phosphohistidine (e.g., via hydrolysis) or any cross-transfer to noncognate response regulators. Consistently, transfers of phosphoryl groups from sensors to response regulators are known to be faster than sensor autophosphorylations (56). Once CusR becomes phosphorylated, it can then dissociate from CusS (Fig. 4, step *v*) and may further dimerize before binding chromosomal operator site for gene activation (Fig. 4, step *vi*).

TCSs are ubiquitous in bacteria and regulate a variety of cellular functions. The mode and timing of CusS–CusR interactions upon sensing the substrate metal should be useful in understanding the mechanisms of other TCSs and helping discover strategies to interfere with the respective cell function for antibacterial treatments.

Materials and Methods

Materials and methods are described in *SI Appendix*, section 1. These include bacterial strain construction, primer design, strain functionality, immunoblotting for intactness of fusion proteins, sample preparation for imaging, SMT and SCQPC procedures, and additional results and analyses. Additional raw data and MATLAB codes have been deposited at Figshare (DOI: 10.6084/m9.figshare.11868639).

ACKNOWLEDGMENTS. This research is supported by NIH Grant GM109993 and in part by Army Research Office Grant W911NF-19-1-0121. L.A.G. is supported by NIH Grants F31AI143208 and 5T32GM008500. We thank Dr. T.-Y. Chen for the development of ITCDD codes; the Cornell University Biotechnology Resource Center for access to the Zeiss LSM880 confocal/multiphoton microscope, supported by New York State Stem Cell Science Program Grant CO29155 and NIH Grant S10OD018516; Y. Aye for access to the immunoblot imaging instrument; B. M. Wendel and J. D. Helmann for inductively coupled plasma mass spectrometry measurements; and M. M. McEvoy for comments.

1. P. Chandrangsu, C. Rensing, J. D. Helmann, Metal homeostasis and resistance in bacteria. *Nat. Rev. Microbiol.* **15**, 338–350 (2017).
2. Z. Ma, F. E. Jacobsen, D. P. Giedroc, Metal transporters and metal sensors: How coordination chemistry controls bacterial metal homeostasis. *Chem. Rev.* **109**, 4644–4681 (2009).
3. K. J. Waldron, J. C. Rutherford, D. Ford, N. J. Robinson, Metalloproteins and metal sensing. *Nature* **460**, 823–830 (2009).
4. C. E. Outten, T. V. O'Halloran, Femtomolar sensitivity of metalloregulatory proteins controlling zinc homeostasis. *Science* **292**, 2488–2492 (2001).
5. H. Reyes-Caballero, G. C. Campanello, D. P. Giedroc, Metalloregulatory proteins: Metal selectivity and allosteric switching. *Biophys. Chem.* **156**, 103–114 (2011).
6. A. Gaballa, J. D. Helmann, Identification of a zinc-specific metalloregulatory protein, Zur, controlling zinc transport operons in *Bacillus subtilis*. *J. Bacteriol.* **180**, 5815–5821 (1998).
7. C. P. Zschiedrich, V. Keidel, H. Szurmant, Molecular mechanisms of two-component signal transduction. *J. Mol. Biol.* **428**, 3752–3775 (2016).
8. K. Yamamoto, A. Ishihama, Transcriptional response of *Escherichia coli* to external copper. *Mol. Microbiol.* **56**, 215–227 (2005).
9. G. Grass, C. Rensing, Genes involved in copper homeostasis in *Escherichia coli*. *J. Bacteriol.* **183**, 2145–2147 (2001).
10. F. W. Outten, D. L. Huffman, J. A. Hale, T. V. O'Halloran, The independent cue and cus systems confer copper tolerance during aerobic and anaerobic growth in *Escherichia coli*. *J. Biol. Chem.* **276**, 30670–30677 (2001).
11. J. M. Argüello, D. Raimunda, T. Padilla-Benavides, Mechanisms of copper homeostasis in bacteria. *Front. Cell. Infect. Microbiol.* **3**, 73 (2013).
12. T. Affandi, A. V. Issaian, M. M. McEvoy, The structure of the periplasmic sensor domain of the histidine kinase CusS shows unusual metal ion coordination at the dimeric interface. *Biochemistry* **55**, 5296–5306 (2016).
13. G. P. Munson, D. L. Lam, F. W. Outten, T. V. O'Halloran, Identification of a copper-responsive two-component system on the chromosome of *Escherichia coli* K-12. *J. Bacteriol.* **182**, 5864–5871 (2000).
14. T. Affandi, M. M. McEvoy, Mechanism of metal ion-induced activation of a two-component sensor kinase. *Biochem. J.* **476**, 115–135 (2019).
15. S. A. Gudipaty, A. S. Larsen, C. Rensing, M. M. McEvoy, Regulation of Cu(I)/Ag(I) efflux genes in *Escherichia coli* by the sensor kinase CusS. *FEMS Microbiol. Lett.* **330**, 30–37 (2012).
16. T. D. Mealman, N. J. Blackburn, M. M. McEvoy, Metal export by CusCFBA, the periplasmic Cu(I)/Ag(I) transport system of *Escherichia coli*. *Curr. Top. Membr.* **69**, 163–196 (2012).
17. A. M. Stock, V. L. Robinson, P. N. Goudreau, Two-component signal transduction. *Annu. Rev. Biochem.* **69**, 183–215 (2000).
18. S. J. Cai, M. Inouye, EnvZ-OmpR interaction and osmoregulation in *Escherichia coli*. *J. Biol. Chem.* **277**, 24155–24161 (2002).
19. A. Stock, T. Chen, D. Welsh, J. Stock, CheA protein, a central regulator of bacterial chemotaxis, belongs to a family of proteins that control gene expression in response to changing environmental conditions. *Proc. Natl. Acad. Sci. U.S.A.* **85**, 1403–1407 (1988).
20. E. A. Groisman, The pleiotropic two-component regulatory system PhoP-PhoQ. *J. Bacteriol.* **183**, 1835–1842 (2001).
21. K. Singh, D. B. Senadheera, D. G. Cvitkovitch, An intimate link: Two-component signal transduction systems and metal transport systems in bacteria. *Future Microbiol.* **9**, 1283–1293 (2014).
22. H. Urano *et al*., Cross-regulation between two common ancestral response regulators, HprR and CusR, in *Escherichia coli*. *Microbiology* **163**, 243–252 (2017).
23. G. Rivera-Cancel, W. H. Ko, D. R. Tomchick, F. Correa, K. H. Gardner, Full-length structure of a monomeric histidine kinase reveals basis for sensory regulation. *Proc. Natl. Acad. Sci. U.S.A.* **111**, 17839–17844 (2014).
24. Y. Gambin *et al*., Lateral mobility of proteins in liquid membranes revisited. *Proc. Natl. Acad. Sci. U.S.A.* **103**, 2098–2102 (2006).
25. D. Lucena, M. Mauri, F. Schmidt, B. Eckhardt, P. L. Graumann, Microdomain formation is a general property of bacterial membrane proteins and induces heterogeneity of diffusion patterns. *BMC Biol.* **16**, 97 (2018).
26. M. Koler, V. Frank, H. Amartely, A. Friedler, A. Vaknin, Dynamic clustering of the bacterial sensory kinase BaeS. *PLoS One* **11**, e0150349 (2016).
27. J. J. Sieber *et al*., Anatomy and dynamics of a supramolecular membrane protein cluster. *Science* **317**, 1072–1076 (2007).
28. L. Johannes, W. Pezeshkian, J. H. Ipsen, J. C. Shillcock, Clustering on membranes: Fluctuations and more. *Trends Cell Biol.* **28**, 405–415 (2018).
29. S. A. Gudipaty, M. M. McEvoy, The histidine kinase CusS senses silver ions through direct binding by its sensor domain. *Biochim. Biophys. Acta* **1844**, 1656–1661 (2014).
30. M. Zhang *et al*., Rational design of true monomeric and bright photoactivatable fluorescent proteins. *Nat. Methods* **9**, 727–729 (2012).
31. J. Elf, G.-W. Li, X. S. Xie, Probing transcription factor dynamics at the single-molecule level in a living cell. *Science* **316**, 1191–1194 (2007).
32. T.-Y. Chen *et al*., Concentration- and chromosome-organization-dependent regulator unbinding from DNA for transcription regulation in living cells. *Nat. Commun.* **6**, 7445 (2015).
33. F. Oswald, E. L M Bank, Y. J. M. Bollen, E. J. G. Peterman, Imaging and quantification of trans-membrane protein diffusion in living bacteria. *Phys. Chem. Chem. Phys.* **16**, 12625–12634 (2014).
34. T.-Y. Chen *et al*., Quantifying multistate cytoplasmic molecular diffusion in bacterial cells via inverse transform of confined displacement distribution. *J. Phys. Chem. B* **119**, 14451–14459 (2015).
35. A. G. Santiago *et al*., Adaptor protein mediates dynamic pump assembly for bacterial metal efflux. *Proc. Natl. Acad. Sci. U.S.A.* **114**, 6694–6699 (2017).
36. P. E. Schavemaker, A. J. Boersma, B. Poolman, How important is protein diffusion in prokaryotes? *Front. Mol. Biosci.* **5**, 93 (2018).
37. C. W. Mullineaux, A. Nenninger, N. Ray, C. Robinson, Diffusion of green fluorescent protein in three cell environments in *Escherichia coli*. *J. Bacteriol.* **188**, 3442–3448 (2006).
38. N. Zahid, S. Zulfiqar, A. R. Shakoori, Functional analysis of cus operon promoter of *Klebsiella pneumoniae* using *E. coli* lacZ assay. *Gene* **495**, 81–88 (2012).
39. M. A. Moran *et al*., Sizing up metatranscriptomics. *ISME J.* **7**, 237–243 (2013).
40. A. L. Koch, H. R. Levy, Protein turnover in growing cultures of *Escherichia coli*. *J. Biol. Chem.* **217**, 947–957 (1955).
41. J. Mandelstam, Turnover of protein in growing and non-growing populations of *Escherichia coli*. *Biochem. J.* **69**, 110–119 (1958).
42. E. Borek, L. Ponticorvo, D. Rittenberg, Protein turnover in microorganisms. *Proc. Natl. Acad. Sci. U.S.A.* **44**, 369–374 (1958).
43. J. C. M. Gebhardt *et al*., Single-molecule imaging of transcription factor binding to DNA in live mammalian cells. *Nat. Methods* **10**, 421–426 (2013).
44. J. Rocha, J. Corbitt, T. Yan, C. Richardson, A. Gahlmann, Resolving cytosolic diffusive states in bacteria by single-molecule tracking. *Biophys. J.* **116**, 1970–1983 (2019).
45. S. Uphoff, R. Reyes-Lamothe, F. Garza de Leon, D. J. Sherratt, A. N. Kapanidis, Single-molecule DNA repair in live bacteria. *Proc. Natl. Acad. Sci. U. S. A.* **110**, 8063–8068 (2013).
46. Y. Liao, J. W. Schroeder, B. Gao, L. A. Simmons, J. S. Biteen, Single-molecule motions and interactions in live cells reveal target search dynamics in mismatch repair. *Proc. Natl. Acad. Sci. U.S.A.* **112**, E6898–E6906 (2015).
47. K. Yamamoto *et al*., Functional characterization in vitro of all two-component signal transduction systems from *Escherichia coli*. *J. Biol. Chem.* **280**, 1448–1456 (2005).
48. J.-S. Seok, S. Kaplan, J.-I. Oh, Interacting specificity of a histidine kinase and its cognate response regulator: The PrrBA system of *Rhodobacter sphaeroides*. *Microbiology* **152**, 2479–2490 (2006).
49. H.-N. Lee *et al*., Involvement of the catalytically important Asp54 residue of *Mycobacterium smegmatis* DevR in protein-protein interactions between DevR and DevS. *FEMS Microbiol. Lett.* **343**, 26–33 (2013).

50. G. S. Lukat, B. H. Lee, J. M. Mottonen, A. M. Stock, J. B. Stock, Roles of the highly conserved aspartate and lysine residues in the response regulator of bacterial chemotaxis. *J. Biol. Chem.* **266**, 8348–8354 (1991).
51. L. Bellsolell, J. Prieto, L. Serrano, M. Coll, Magnesium binding to the bacterial chemotaxis protein CheY results in large conformational changes involving its functional surface. *J. Mol. Biol.* **238**, 489–495 (1994).
52. Y. Wen *et al*., Mechanistic insight into how multidrug resistant *Acinetobacter baumannii* response regulator AdeR recognizes an intercistronic region. *Nucleic Acids Res.* **45**, 9773–9787 (2017).
53. G. L. Draughn *et al*., The structure of the biofilm-controlling response regulator BfmR from *Acinetobacter baumannii* reveals details of its DNA-binding mechanism. *J. Mol. Biol.* **430**, 806–821 (2018).
54. I. G. Janausch, I. Garcia-Moreno, D. Lehnen, Y. Zeuner, G. Unden, Phosphorylation and DNA binding of the regulator DcuR of the fumarate-responsive two-component system DcuSR of *Escherichia coli*. *Microbiology* **150**, 877–883 (2004).
55. A. K. Eaton, R. C. Stewart, Kinetics of ATP and TNP-ATP binding to the active site of CheA from *Thermotoga maritima*. *Biochemistry* **49**, 5799–5809 (2010).
56. M. P. Bhate, K. S. Molnar, M. Goulian, W. F. DeGrado, Signal transduction in histidine kinases: Insights from new structures. *Structure* **23**, 981–994 (2015).
57. A. D. Gutu, K. J. Wayne, L.-T. Sham, M. E. Winkler, Kinetic characterization of the WalRKSpn (VicRK) two-component system of *Streptococcus pneumoniae*: Dependence of WalKSpn (VicK) phosphatase activity on its PAS domain. *J. Bacteriol.* **192**, 2346–2358 (2010).
58. S. L. Fisher, S.-K. Kim, B. L. Wanner, C. T. Walsh, Kinetic comparison of the specificity of the vancomycin resistance VanSfor two response regulators, VanR and PhoB. *Biochemistry* **35**, 4732–4740 (1996).